Journal of Energy Storage 59 (2023) 106458

Contents lists available at ScienceDirect

Journal of Energy Storage

journal homepage: www.elsevier.com/locate/est

Research papers

Battery lifetime of electric vehicles by novel rainflow-counting algorithm with temperature and C-rate dynamics: Effects of fast charging, user habits, vehicle-to-grid and climate zones

Davide Fioriti [a,*], Claudio Scarpelli [a], Luigi Pellegrino [b], Giovanni Lutzemberger [a], Enrica Micolano [b], Sara Salamone [a,b]

[a] DESTEC, University of Pisa, Largo Lucio Lazzarino 1, Pisa, 56122, Italy
[b] Ricerca sul Sistema Energetico, Via Rubattino 54, Milano, 20134, Italy

ARTICLE INFO

Keywords:
Hybrid Electric Vehicles (HEV)
Lithium Battery Energy Storage System (BESS)
Smart charging
Long-term battery storage degradation
Battery capacity fading
State of Health (SoH)

ABSTRACT

The adoption of electric vehicles is expected to soon widespread to cope with energy transition needs; however, concerns on battery lifetime arise, especially related to charging behaviors, vehicle usage habits, vehicle-to-grid and weather conditions. In fact, lifetime battery modeling is a challenging dynamic to characterize, as it involves complex chemical processes related to charging, discharging and temperature dynamics over long time spans that are often difficult to dominate, given the large uncertainties. Having a fatigue-like behavior, the battery aging has sometimes been modeled using rainflow-counting algorithms, yet traditional modeling is not holistic and approximations are used, especially when considering temperature or current dynamics. Based on experimental data, this paper aims at developing a holistic battery degradation model based on rainflow-counting algorithm to properly account for all major determinants of capacity loss, namely cycling usage, calendar lifetime, dynamic temperature and battery current. The approach is coupled with a physical-electro-thermal modeling of the vehicle system, developed in Modelica language, to accurately simulate the intertwined thermal and electrical behavior of the system subject to different usage charging behaviors, including slow and fast charging, as well as vehicle-to-grid application. The proposed case study shows the expected lifetime of electric vehicles to be comparable with of traditional cars (10–20y) and that the proposed temperature-dependent battery modeling enables reducing estimation errors up to 27%. A sensitivity on different climate zones has been considered and results suggest that cool climates can increase life expectancy by 30% with respect to hot climates in typical Italian contexts.

1. Introduction

1.1. Motivation

Electromobility is now enjoying a renewed interest due to the increased attention towards environmental issues, so the penetration of electric vehicles is now beginning, at last. However, the so-called "range anxiety" [1], the different usage patterns, e.g. commuter or highway, different weather conditions and charging rate [2] are all concerns that are affecting the acceptance of the technology, as they lead to uncertainties in the lifetime of batteries that is a critical element for consumers. On the other hand, models for the battery lifetime estimation are anything but a known science: several techniques have been proposed but the significant chemical-dependent properties, the physical processes and the various stresses the batteries are subject to make battery estimation a very complex task. Range anxiety can be reduced by implementing fast charging options, yet they can have a toll on battery lifetime; weather conditions can affect the operating temperature of the battery, in agreement to the cooling system of the vehicle, and the typical operating conditions of the vehicle, e.g. urban or extra-urban contexts, can reduce the expected lifetime as well. Combining all these factors is complex and rarely it has been addressed in the literature.

In this study, we propose a methodology to estimate the expected life of vehicular batteries subject by using a novel battery degradation model to account for all the relevant degradation factors mentioned above. Based on existing literature and experimental tests, a novel battery degradation model is discussed and used to estimate the life-time of electric batteries subject to various cycling operation, charging

* Corresponding author.
E-mail address: davide.fioriti@unipi.it (D. Fioriti).

https://doi.org/10.1016/j.est.2022.106458
Received 20 May 2022; Received in revised form 4 November 2022; Accepted 16 December 2022
Available online 29 December 2022

patterns, vehicle-to-grid and weather conditions. A case study using realistic Italian usage patterns and weather conditions is proposed. The methodology is expected to advice policy makers, companies and scientists on modeling techniques for battery estimation and suggesting that expected electric vehicle lifetimes are already comparable to traditional fuel-powered cars.

1.2. Battery degradation

Given the paramount importance of batteries for achieving the energy transition, battery modeling and degradation have been extensively studied to characterize physical, thermal and chemical properties [3,4], especially for vehicle applications [5], for operation and planning purposes. Future research is ongoing and novel chemistries have been proposed with strong potential [6], though currently lithium-ion batteries systems are expected to dominate the market [5,7] and in this study we focus on their modeling.

The literature is rich of both theoretical and empirical approaches. In theoretical models, chemical properties of materials and diffusion dynamics are accurately described to derive numerical or mathematical models [8]. These models are usually very complex as they require a large number related to parameters of the materials, the construction process and geometries, that are often unknown and hard to compute [9]; moreover, the physics and chemistry theory involve complex equations to handle. Empirical approaches tend to be simpler but they require the execution of several tests lasting several months to properly capture the degradation dynamics of batteries subject to different types of stress [10,11]: temperature, current, cycling operation and calendar life, or time [12]. Once the measurements have been performed, a numerical model is fitted over the experimental results to reproduce the measured degradation dynamics. Hybrid models, instead, lay in the between: they are generally empirical models that partially inherit the physics of the degradation by using fitting functions that resemble theoretical diffusion functions, properties of materials or speed of reactions, such as the Arrhenius function that is well known in chemistry [13,14]. Given these properties, hybrid models can reduce the need for experimental tests, as theoretical knowledge improves the fitting rate of the model, and improve the overall accuracy. For these reasons, in this study we focus on hybrid models.

The battery aging can be described as the superimposition of different degradation factors, namely time, temperature, and the operating power profile, which are usually grouped into two categories [15,16]: the so-called calendar life, referring to the aging effect involving time, and cycle life, related to the cyclical operating conditions of the battery; temperature conditions affect the degradation rate of both. Traditional empirical techniques are based on simple polynomial fitting to capture the nexus between a single aging factor and the capacity degradation [9], such as the State-of-Charge (SoC) [17], Depth-of-Discharge (DoD) [10], or the temperature; rarely they consider the combined effect of multiple degradation factors. Better performances could be achieved by hybrid models that use function shapes inherited by theory, such as the Arrhenius [13,14], to characterize the cycling aging of batteries [18], also when subject to variable conditions [19].

According to the literature, the battery degradation can be characterized by fatigue-related dynamic in which the application of diversified and repetitive stresses lead to the reduction of the State-of-Health (SoH), similarly to mechanics [20]. In this view, some studies have considered not only the cycling operation of charging/discharging behaviors [10] but also the combinations of multiple stresses [19,21,22]. The study in [19] proposed the calculation of the degradation by using an iterative approach to account for the cycling operation and temperature degradation, also including the Arrhenius equation. In [22], inspired by the exponential function well used in the Arrhenius equation, the authors proposed a weighted-sum approach to account for the cycling operation using exponential and logarithmic functions, modeled as a function of the average SoC and its standard deviation, and the temperature. Again, also in [22], the Arrhenius function has been used to model the temperature-related dynamics. Moreover, the hybrid methodology described in [23], inspired by [21], proposes a rainflow-based methodology to capture the combined effects of cycling, temperature effects and calendar life by using a modified Arrhenius function, logarithmic/exponential fitting for combining different stresses and polynomial fitting to characterize specific phenomena of the battery degradation. The rainflow-counting algorithm, used in mechanical standards to quantify fatigue [24], identifies the cycling operation of the battery, whereas a customized function to model calendar aging keeps track of the dynamics related to time. Given the ability of the model to characterize various degradation phenomena, this approach has been considered and improved in this study.

1.3. Battery thermal model

Battery degradation is significantly affected by its temperature. The evolution of the battery temperature depends on the ambient temperature as well as the battery working condition. Indeed, EV battery pack systems can produce high amounts of heat (e.g., during fast charging process), which increase the battery temperature, directly affecting battery performance, lifetime and safety [2]. To consider this aspect, the analysis performed include a battery thermal model.

Several thermal models have been presented in literature, i.e. electrochemical–thermal coupled model, electro-thermal coupled model, thermal abuse model, 1D model, 2D model, 3D model, etc. [25,26]. The first two models (electrochemical–thermal and electro-thermal model) are more common than the others because they can calculate battery external characteristics such as charge–discharge curves and temperature distributions [27]. Electrochemical–thermal models analyze the influence of electrochemical parameters on thermal properties taking into consideration the cell materials, yet they require a large number of electrochemical parameters [28]. In contrast, electro-thermal models adopt empirical equations focusing on the electrical properties of the cell. They require fewer parameters and less calculation [29]. The need for a low computational burden lead us to choose electro-thermal model.

1.4. Battery lifetime of electric vehicles

The lifetime of an electric vehicle battery is deeply influenced by several aspects related to the way the vehicle is used, such as the driving pattern, the acceleration pattern, the charging habits, and even the ambient temperature [30,31]. All these factors impact the battery life through different degradation phenomena, which are reflected into a progressively decay of the vehicle overall performances, the most important of which is the available driving range, caused by a progressively degradation of the battery capacity over time. As a de-facto rule, the life of an EV battery is considered to have reached its End-of-Life (EoL) as soon as its available capacity drops below the threshold of the 80% of what is called the Beginning-of-Life (BoL) capacity. To quote one meaningful example which shows how the lifetime of a battery could be deeply affected by the use of the vehicle it is installed in, Lehtola et al. [32] have highlighted that when a battery is cycled with a DoD of only 5%, an expected lifetime of more than 20 years is guaranteed; on the contrary, when the same battery is cycled with a DoD of 80%, the expected lifetime drops to no more than 10 years. Moreover, Saldaña et al. [33] have concluded that driving environment plays a key role in determining the degradation of EV batteries. Specifically, urban driving scenarios show around 75% longer lifetime than highway driving scenarios, because of the greater power needed, which reflects in greater C-rate the battery is subjected to and deeper discharging rates. In addition, charging power rate has been analyzed as well, displaying that, when compared with a 22 kW rate recharge power, a 7-kW rate extends battery life by around 50%,

while a 43-kW one reduces the battery life of about 12%. Anyhow, one important fact which these studies agree on is that even for the highest stressed batteries analyzed, the expected lifetime still remains beyond the typical battery lifespans guaranteed by EV manufacturers, which appear aligned around 8 years. Indeed, Volkswagen ID3 battery is guaranteed for 8 years or 160 10^3 km [34], Tesla model S and X are guaranteed for 8 years and 257 10^3 km (150 10^3 miles) [35], while 8 years and 160 10^3 km are available for Renault Zoe [36].

1.5. Main contributions

According to the proposed literature analysis and to the authors' best knowledge, the main contributions of this paper are listed below:

1. Development of a battery degradation model based on rainflow-counting algorithm to account for calendar and cycling aging, cold environments, C-rate degradation effects, and dynamic temperature cycling and calendar aging, also with extensive resting periods; the model has been calibrated using experimental aging tests.
2. Estimation of the battery lifetime subject to different electric vehicle behaviors, fast charging and vehicle-to-grid (V2G) applications.
3. Evaluation of different weather conditions impact on the lifetime of vehicles' batteries.
4. Italian case study.

1.6. Organization

Section 2 describes the methodology for vehicle modeling and the battery degradation, Section 3 details the case study and Section 4 reports the results. Finally, the conclusions are drawn.

2. Battery degradation model by physical-thermo-electrical simulations

2.1. The approach

Fig. 1 describes the procedure used to perform the complete physical -electrical modeling to simulate the battery degradation of the vehicle system with an holistic approach. In particular, after a preliminary processing of the major inputs of the vehicle characteristics, the usage pattern and the weather conditions, an iterative approach is executed to simulate each day of operation at hourly time resolution. The physical modeling is captured by using a detailed model developed in Modelica language [37] that aims at capturing the mechanical dynamics of the vehicle and the electrical and thermal behavior of the battery, given the vehicle usage pattern and the weather condition of each simulated day d. The SoC profile and the battery temperature calculated by the model are then used by the proposed rainflow-based battery degradation model to estimate the battery capacity after each time step (1 s). The procedure is iterated until EoL is reached.

To reduce computational requirements, especially considering the complex thermal, electrical and physical model of the hybrid vehicle model, the weather data have been clustered into N days, which enables pre-processing the load profiles and reduce the computational burden of the analysis.

2.2. Vehicle model

One of the objectives of the present study consists in assessing the influence of the driving patterns over the battery operation. To this aim, a numerical simulation model has been developed, as reported in Fig. 2. The considered vehicle model comprehends different sub-parts: the driver model, the mechanical model, the electric drive, and the storage system.

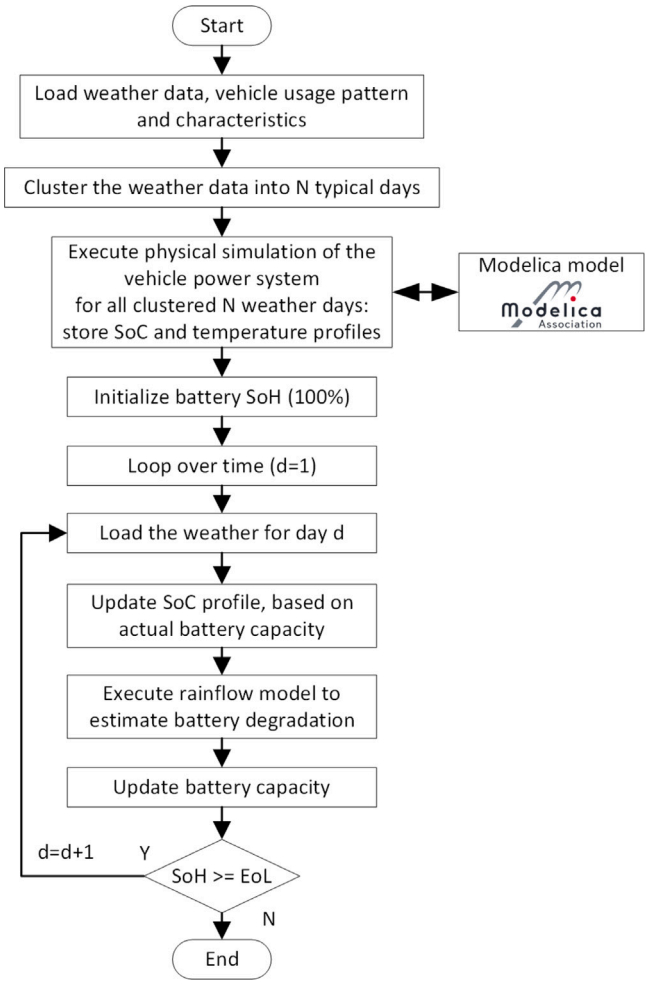

Fig. 1. The holistic physical-electrical-thermal approach to model battery degradation.

The driver model is implemented as a proportional speed controller that outputs the motor torque (traction or braking) required to follow an input driving cycle. The mechanical part models the longitudinal dynamic of the vehicle according to (1), where m_{eq} is the equivalent inertia of the vehicle, F_x is the resistance force, F_{torque} is the longitudinal force derived from the application to the wheels of the electric machine torque, through a gear ratio, and $\ddot{x}$ is the longitudinal acceleration that is the second derivative of the longitudinal distance x traveled by the vehicle.

$$F_{torque} - F_x = m_{eq} \cdot \ddot{x}, \tag{1}$$

The resistance force F_x, in flat condition, is composed of the rolling resistance and the aerodynamics drag. Accordingly, it is calculated in (2), where m_{eq} is the vehicle mass, g the gravitational acceleration, f_0 the rolling resistance coefficient, ρ the air density, S the frontal area, C_x the aerodynamic coefficient, and $\dot{x}$ is the linear speed of the vehicle, calculated as the first derivative of the linear distance x traveled by the vehicle.

$$F_x = m_{eq} \cdot g \cdot f_0 + \frac{1}{2} \rho \cdot C_x \cdot S \cdot \dot{x}^2, \tag{2}$$

The electric drive, which consists of the electric machine and the relative power converter, is modeled as being algebraic, i.e. with maps containing operating efficiency and regions. Since the powertrain dynamics are slower than the electric ones, the only dynamic considered is the mechanical dynamic related with the mechanical inertia of the rotating parts, while the electrical dynamics have been neglected. Thus,

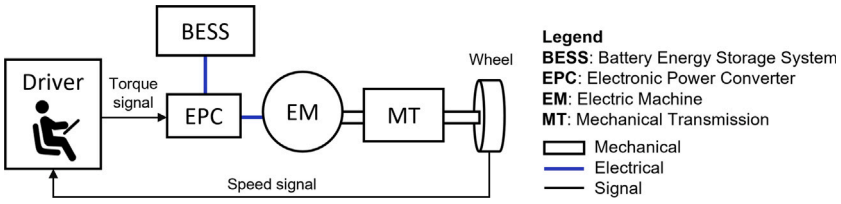

Fig. 2. Conventional power train scheme.

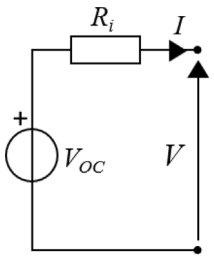

Fig. 3. Equivalent circuit model of the battery system.

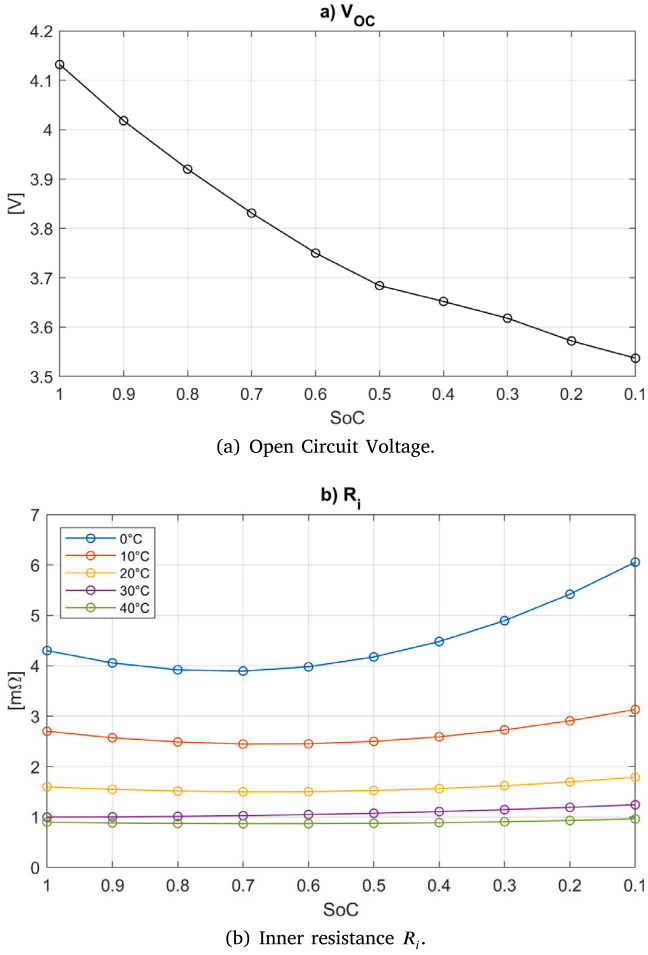

(a) Open Circuit Voltage.

(b) Inner resistance R_i.

Fig. 4. (a) Open Circuit Voltage as a function of the SoC; (b) Inner resistance R_i as a function of the SoC and the temperature.

the electric drive applies the mechanical torque requested from the driver to the inertia. The applied torque and the speed determine the operating point of the electric drive, which is used in an efficiency map to calculate the drive losses. This approach has been verified by the authors in [38,39], proving that average errors of the model can be below 5% with respect to experimental data. Moreover, for the present study, the efficiency maps of the electric drive have been tuned in order to align the energy consumption of the simulated vehicle to the today standards of main EV manufactures, as further specified in Section 3.3. As shown in Fig. 3, the storage system is modeled by an equivalent electric circuit composed of an electromotive force and an inner resistance. The electromotive force is parameterized by the Open Circuit Voltage (V_{oc}) as a function of the SoC, relationship that is depicted in Fig. 4(a) based on the experimental testing procedure described in Section 3.4. The value of the inner resistance (R_i) is calculated as a function of the SoC and the temperature, according to the trend reported in Fig. 4(b). Although much more sophisticated battery models exist, which include the dynamic behavior of the main electrical phenomena occurring inside the battery itself (as already investigated by the same authors in [40] and widely in literature [41]), given the goal of this paper, we considered a static battery electrical model as a trade-off between accuracy and computational time. The detailed reasons are the following: (a) for the purpose of the present paper, we are not interested in the internal electrical dynamics of the battery, because they are in the order of minutes, while the time horizon of our simulations is in the order of days, and (b) the static-algebraic model of Fig. 3 includes all the major elements to capture the thermal model equations: indeed, the model with a single resistance parameter R_i enables representing the temperature dynamics of the battery with an acceptable error, as demonstrated in [42].

The thermal model of the EV battery pack has been developed starting from the equation of the heat generation rate model proposed by Bernardi [43]: an energy balance is applied to estimate the battery temperature. Assuming that the thermal distribution inside the cell is uniform and that the conduction resistance inside the battery cell is negligible compared with the convection and radiation heat transfer [44], the temperature variation depends on the battery thermal capacity (C_p) and the difference between the generated heat and the dissipated heat. Generated heat comprises two sources, irreversible heat generation by means of the effective ohmic resistance of the cell's material, and reversible generated heat due to the entropy change in both cathode and anode. The total entropy changes in the battery cell can be considered as zero according to [45]. According to [46], assuming that the temperature differences between the cells in the single battery module are small, the battery temperature behavior can be described with (3). ΔT is the difference between the battery cell (T^B) and the ambient temperatures (T^A), h is the natural convection coefficient, M is the total battery mass, and I^B is the battery current. R_i is the battery internal resistance shown in Fig. 2 which generates heat, A is the surface area of the cells blocks in the single battery module, σ is Stefan–Boltzmann constant, and ϵ is the emissivity of heat.

$$M \cdot C_p \cdot \frac{dT^B}{dt} = R_i \cdot I^{B^2} - h \cdot A \cdot \Delta T - \epsilon \cdot \sigma \cdot A \cdot (T^{B^4} - T^{A^4}) \tag{3}$$

In particular, Saw et al. [47] has pointed out to the contribution of the contact resistance in heat generation, yet when the cell connectors are welded, as considered in this study, the contact resistance can be neglected.

2.3. The battery degradation model

2.3.1. Description

The model proposed in this activity improves the methodologies discussed in [21,48] by (a) improving the representation of battery degradation at low temperatures, (b) considering time-variable temperature profiles, (c) including the cycling degradation at microcyles with low DoD and (d) modeling the C-rate dependency of capacity degradation. The mathematical modeling of the battery degradation is reported in (4)–(6).

Eqs. (4) and (5) clarify the actual value of the battery capacity $E_t^{B,A}$ for every time step t, where ξ_t represents the specific degradation rate. Expression (5) clarifies that the degradation rate is an exponential function of the linearized degradation variable f_t^d, with parameters α^{sei} and β^{sei} that model the degradation effects related to the initial creation of the solid-electrolyte interphase (sei), both being zero for modeling used batteries [21]. Similarly to [48], f_t^d is modeled with (6) as the sum of the contributes due to the calendar aging ($f_{s,\tau}^{d,cal}$) and the cycling aging ($f_r^{d,cyc}$), however, their complete expressions have been significantly improved as detailed in the following subsections.

$$E_t^{B,A} = \left(1 - \xi_{t-1}\right) \cdot E_i^{B,N} \tag{4}$$

$$\xi_t = 1 - \alpha^{sei} \cdot e^{-\beta^{sei} \cdot f_t^d} - \left(1 - \alpha^{sei}\right) \cdot e^{-f_t^d} \tag{5}$$

$$f_t^d = \sum_{s \in N^S, \tau \in N^T} f_{s,\tau}^{d,cal} + \sum_{r \in N^R} f_r^{d,cyc} \tag{6}$$

2.3.2. Calendar life degradation

The calendar aging, modeled using (7), aims at modeling the main degradation phenomena related to the calendar degradation: time, temperature and average SoC. Its mathematical description is characterized by several non-linear functions here detailed: $S^t(\Delta_{s,\tau})$ describes the degradation effect related to the time since installation, $S^\sigma(\sigma_{s,\tau})$ denotes the aging due to the SoC, $S^{T,cal}(T_{s,\tau}^B)$ describes the accelerated degradation due to temperature. With respect to the literature [21,48], the traditional calendar aging model has been improved by including (a) combined degradation of SoC and temperature and (b) a matrix-like approach to quantify the main degradation stresses ($\Delta_{s,\tau}^B$, $\sigma_{s,\tau}$ and $T_{s,\tau}^B$), as shown in Fig. 5.

$$f_{s,\tau}^{d,cal} = S^\sigma(\sigma_{s,\tau}) \cdot S^t(\Delta_{s,\tau}^B) \cdot S^{T,cal}(T_{s,\tau}^B(T^A, I^B)) \tag{7}$$

The first novelty of the methodology relates to the modeling of the calendar life to account for the non-linear dynamic behavior of both temperature and SoC, which were missing in [21,48]. To this goal, the quantities are quantized: the SoC and temperature intervals are divided into intervals and the procedure calculates the duration the battery has been operated in each interval of SoC (s) and temperature (τ). The proposed matrix structure is sketched in Fig. 5 to clarify the approach and the mathematical formulation is reported in (8)–(10), which quantifies respectively the duration $\Delta_{s,\tau}^B$, the average temperature $T_{s,\tau}^B$ and SoC $\bar{\sigma}_{s,\tau}^B$ the battery system operates in the temperature interval τ, delimited by $T_\tau^{B,max/min}$, and SoC interval s, delimited by $SoC_s^{max/min}$.

$$T_{s,\tau}^B = \text{mean}\left(\left\{T_t^B : T_t^B \in \left[T_\tau^{B,min}, T_\tau^{B,max}\right], SoC_t \in \left[SoC_s^{min}, SoC_s^{max}\right], \forall t\right\}\right) \tag{8}$$

$$\sigma_{s,\tau} = \text{mean}\left(\left\{SoC_t : T_t^B \in \left[T_\tau^{B,min}, T_\tau^{B,max}\right], SoC_t \in \left[SoC_s^{min}, SoC_s^{max}\right], \forall t\right\}\right) \tag{9}$$

$$\Delta_{s,\tau}^B = \text{sum}\left(\left\{\Delta t : T_t^B \in \left[T_\tau^{B,min}, T_\tau^{B,max}\right], SoC_t \in \left[SoC_s^{min}, SoC_s^{max}\right], \forall t\right\}\right) \tag{10}$$

Finally, Eqs. (11), (12) and (13) depict the calendar degradation effects due to temperature, the average SoC and time, respectively. With respect to [21,48], the formulations have been improved to account for conjoint temperature and SoC dynamics. k^T, k^t, k^σ are experimental coefficients that can be tailored with the procedure described in [21], and T_{ref}^B and $sigma^{ref}$ are reference temperature (25 °C) and reference SoC (50%) used to perform the experimental calibration of the before-mentioned coefficients.

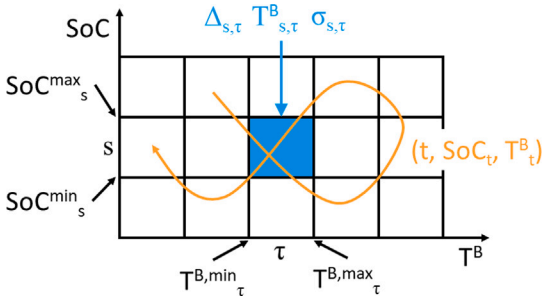

Fig. 5. Matrix structure to capture the temperature-SoC-time dynamics. The orange curve represents the evolution of SoC and temperature over time, and the blue square represents an arbitrary cell in which values are averaged according to the time the system operates in that region, as detailed in (8)–(10).

$$S^{T,cal}(T_{s,\tau}^B) = e^{k^T \cdot \left(T_{s,\tau}^B - T_{ref}^B\right) \cdot \frac{T_{ref}^B}{T_{s,\tau}^B}} \tag{11}$$

$$S^\sigma(\sigma_{s,\tau}) = e^{k_\sigma \cdot (\sigma_{s,\tau} - \sigma_{ref})} \tag{12}$$

$$S^t(\Delta_{s,\tau}) = k^t \cdot \Delta_{s,\tau} \tag{13}$$

2.3.3. Cycle life degradation

The cycling degradation is instead modeled using (14), which is a non-linear function that accounts for DoD ($S^\delta(\delta_r)$), average SoC ($S^\sigma(\sigma_r)$), and temperature $S^{T,cyc}(T_r^B)$ of each cycle of operation calculated using a rainflow counting procedure [24]. Conversely to [21,48], the proposed model accounts for (a) degradation dynamics at low battery temperature, by using a modified function $S^{T,cyc}(T_r^B)$, (b) an accurate modeling of the operating temperature of each degradation cycle, by using a weighted average procedure that also enables avoiding idling periods, and (c) the C-rate degradation dynamics by modeling the battery temperature T_r^B using the physical-electro-thermal model in Section 2.1, which depends on the ambient temperature (T^A) and the battery current (I^B).

$$f_r^{d,cyc} = S^\delta(\delta_r) \cdot S^\sigma(\sigma_r) \cdot S^{T,cyc}(T_r^B(T^A, I^B)) \tag{14}$$

The function $S^\sigma(\sigma_r)$ used to model the degradation effect in (14) is equivalent to the one used in the calendar life in (12), whereas the other formulations are presented below.

As introduced, the proposed approach aims at identifying the average operative temperature that occurred specifically for every battery cycle when the battery was stressed also accounting for the current-related effects that increase the battery temperature, which represent an additional novelty of the study. These temperature-related dynamics have been captured by using the weighted average procedure shown in (15) that quantifies the average temperature the battery is operated at for every rainflow cycle. In the equation, $T^B(T^A, I^B)$ is the temperature of the battery, computed using the physical battery model described in the previous subsection that incorporates the C-rate dynamics, P is the power exchanged with battery (positive when discharging), and T_r denotes the time ranges in which a cycle is active. By using this definition, the procedure successfully identifies the average temperature weighted by the power exchanged with the battery when the battery is operated, thus quantifying the net temperature effect when the charging or discharging stress has occurred, contrary to previous models [21,48]. Note that for every time step t, only a cycle can be active to avoid counting twice the same interval, thus $T_i \cap T_j = \emptyset$, $\forall i, j : i \neq j$.

$$T_r^B = \frac{\int_{t \in T_r} |P| \cdot T^B(T^A, I^B) dt}{\int_{t \in T_r} |P| \, dt} \tag{15}$$

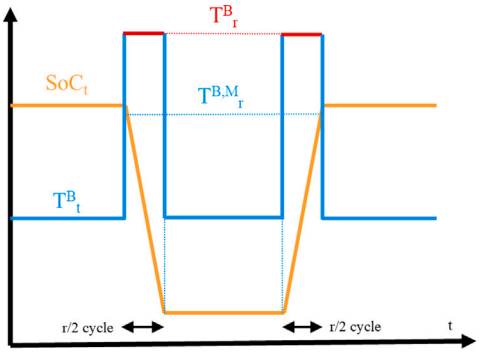

Fig. 6. Methodology to identify conjoint temperature-current dynamics of the cycling degradation.

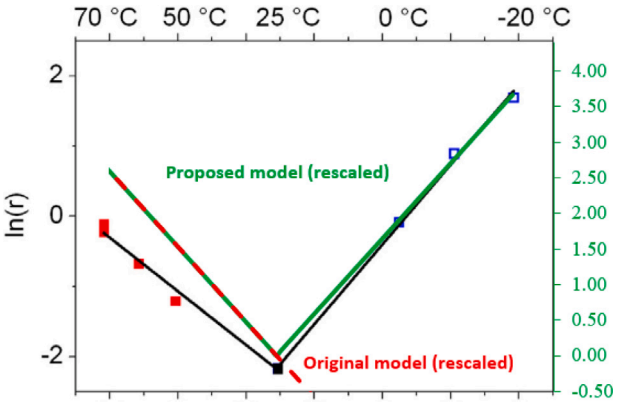

Fig. 7. Comparison of the empirical degradation rates from [49] and the proposed model.
Note: the proposed model discussed in this paper (in green) and the original model (in red) by [21,48] has been re-scaled to be superimposed on the model from [49]. The blue and red dots denote the experimental model from [49]. (For interpretation of the references to color in this figure legend, the reader is referred to the web version of this article.)

To clarify the above, let us consider the battery cycling in Fig. 6 characterized by a first battery discharge, followed by a period of resting and a recharge. In the example, the charging and discharging of the battery occur only at higher temperature, whereas the resting occurs at lower temperature. The proposed procedure successfully obtains the higher temperature value T_r^B as weighted average temperature, whereas traditional approaches based on averaging the temperature between the beginning and end of the cycle, such as [21], would disregard such phenomenon and obtain $T_r^{B,M}$, which is not the net battery temperature when the cycling dynamics occur.

Another improvement relates to characterizing the modeling in cold weathers. In agreement with the literature [50], in cold environments the cycling aging of the battery degrades significantly, similarly to high temperature conditions as studied in [49], yet the original model only considered high temperature phenomena [21,48]. To account for cold environments, in alignment to [49,50], we then propose the modified degradation model as reported in (16), whose parameters are equivalent to those at (13). The overall comparison between the proposed model, the original model in [21,48] and the raw experimental data in [49] is shown in Fig. 7. The figure clearly shows the ability of the proposed approach to capture the dynamics at low temperature, whereas the models in [21,48] cannot.

$$S^{T,cyc}(T_r^B) = e^{k^T \cdot \left|T_r^B - T_{ref}^B\right| \cdot \frac{T_{ref}^B}{T^B}} \tag{16}$$

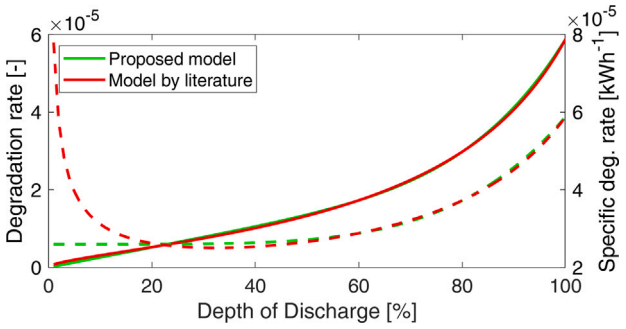

Fig. 8. Comparison of the absolute (solid line) and specific (dashed line) degradation rate of S_δ of the proposed model (in green) with respect to literature [21] (in red). (For interpretation of the references to color in this figure legend, the reader is referred to the web version of this article.)

Another improvement of the cycle life degradation model consists in the appropriate selection of a fitting function to properly describe the degradation rate over the entire range 0%–100% DoD, and in the introduction of appropriate constraints to adhere to experimental data of degradation rates. The proposed DoD effects have been captured using (17), subject to constraint (18) that guarantees that the specific degradation rate at low DoD is a monotone increasing function, conversely to [21]. The authors in [21] calibrated the model at higher DoD ranges (10%–100%), and limited description at low DoD ranges may have lead to lower precision and higher specific degradation rates, whereas the literature suggest lower specific degradation rates in that same range [10]. Fig. 8 compares the proposed model (in green) with the one in [21] (in red) calibrated on the same data and confirms that the proposed approach successfully meets the desired goal. Often, this topic is disregarded, yet it may lead to unexpected behaviors in cycling dynamics with low DoD, which can be critical for energy systems with high renewable penetration, such as for estimating EV battery lifetimes of urban cycles at low DoD (see Section 3).

$$S^\delta(\delta_r) = k^{\delta 1} \cdot \delta_r^{k^{\delta 2}} + k^{\delta 3} \cdot \delta_r \tag{17}$$

$$\frac{\partial \frac{S^\delta(\delta_r)}{\delta_r}}{\partial \delta_r} \geq 0 \tag{18}$$

2.3.4. Calibration of the model

To properly calibrate the model described in this subsection, standard curve fitting tools available in any scientific processing software can be used using the information detailed as follows:

1. Calendar experiments at different temperature. These curves enable calibrating the temperature model and to identify parameters k^T and T_{ref}^B in (11) and (16).
2. Calendar experiments at different SoC. These curves can support the calibration of the SoC dependence parameters k^σ and σ_{ref} of (12).
3. Calendar experiments. The calendar experiments at different temperatures and SoC are then used for calibrating the calendar degradation coefficients k^t of (7).
4. Cycling tests. The traditional curves given by manufacturers that describe the expected lifetime of the battery with respect to the DoD can be used for the calibration of $k^{\delta 1}$, $k^{\delta 2}$ and $k^{\delta 3}$ of (17).

The rational behind these test matrix is that in every testing procedure a single degradation phenomenon is considered at a time and hence it is easy to perform the curve fitting calibration. For example, in calendar tests, only calendar degradation occurs, hence only the left-hand side of (6) contains non-null values. More details on the calibration procedure can be found in [21].

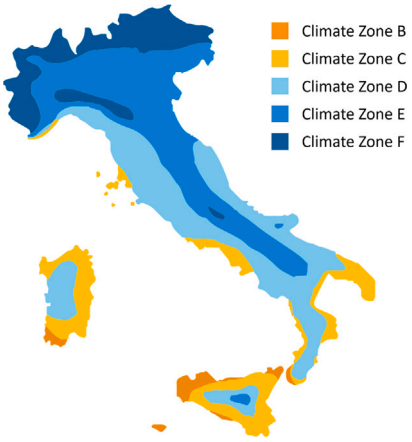

Fig. 9. Italian climate zones.

Table 1
Minimum (min), average (avg) and maximum (max) temperatures for the representative climates by zone.

Zone	Min temp. [°C]	Avg. temp. [°C]	Max. temp. [°C]
B	5.1	18.8	33.0
C	0.5	17.1	35.5
D	−4.0	14.6	33.0
E	−5.7	12.2	30.9
F	−10.8	11.8	32.4

3. Case study

3.1. Description

This section describes the case studies used for performing the technical analysis on the battery lifetime for an Italian case study. The parameters of the electrical and aging model of the battery vehicle are defined according to data based on experiments and previous works. The vehicle characteristics, the charging modes and the vehicle usage have been adapted from the literature in order to highlight the main issues that cause battery degradation and estimate EV battery lifetimes.

3.2. Daily temperatures clustering

The technical analysis takes into account the impact of the ambient temperature, as shown in Fig. 1. In Italy, the weather conditions are usually classified in six climate zones, named from A to F, where A represents the area with the highest temperature and F if the area with the lowest temperature, with the geographical distribution depicted in Fig. 9. The climate zone A, which corresponds to the island Lampedusa in the south of Italy, is not reported, neither considered in the case study because is not representative enough. Aiming to obtain general results for typical Italian conditions, three main weather zones (B, E and F) have been considered that map the majority of the territory. More details on the reference temperature profiles are denoted in Table 1.

Moreover, in order to dominate the computational efforts needed for performing multi-years analysis on several case studies, the yearly temperature data of each climate zone have been clustered into six typical days, as shown in Fig. 1, using *kmeans* algorithm. The ambient temperature profiles of each climate zone have been taken from [51] at 1 h time resolution. As example, Fig. 10 details the clustered six profiles for climate zone F.

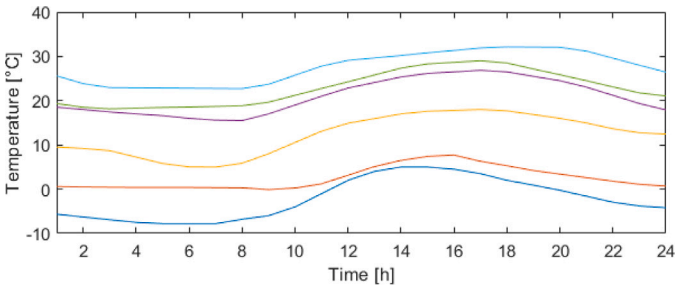

Fig. 10. Temperature profiles of the six typical days for the climate zone F.

3.3. Usage pattern of the hybrid vehicle

The load profile has been selected by considering driving conditions on the standardized WLTC driving cycle [52], which represents typical use conditions in urban, extra-urban roads and highways. In this study, the WLTC has been used to create a typical driving pattern for a commuter (30 km/day) and for a highway driver (500 km/day). The composition and number of repetitions of the WLTC cycle have been selected by analyzing typical characteristics of trips in Italy during 2019, derived from [53]. Main results directly taken from the report have been shown in the following Table 2.

Based on these indicators, four different mission profiles have been defined accordingly. The first three case studies relate to short trips mainly in urban and extra-urban contexts, named as “commuter” usage. In particular, urban and extra-urban portions of the WLTC cycle have been considered, neglecting the highway part. In this way, a road cycle of about 15 km, repeated twice a day to simulate the way forward and the way back, was implemented. After determining the vehicle usage pattern, different charging modes were taken into account. In particular, charging phase was executed according to the following main three options, in order to compare the effects on the battery lifetime. The fourth case is instead a much more stressed long-driving profile, named “highway” usage. All these cases are here listed below:

- Case 1: daily home charging at 3 kW-rated power at the end of every day (vehicle usage: commuter).
- Case 2: public charging located at workplace, at 11 kW of constant rated power, before the return trip to home (vehicle usage: commuter).
- Case 3: public charging located at workplace as before, with the introduction of Vehicle-to-Grid function. In this way, charging profile is different from before, since it is made by multiple charging and discharging phases (vehicle usage: commuter).
- Case 4: vehicle driving on highway at constant speed (120 km/h), with the main goal to cover a full distance of about 500 km. During the trip, at least two fast charging operations are needed, performed at the constant rated power of 120 kW (vehicle usage: highway).

The main characteristics of the vehicle under simulation are shown in the next Table 3. As noticeable, characteristics are of a average medium car, equipped with a typical battery size, nearly about 50 kWh. With this configuration, the simulated vehicle energy consumption under the WLTC standard cycle is 14.8 kWh/100 km, which is in line with the today EV standards [54].

In the activity, all set of temperature profiles have been applied to Case 1, while the other cases have been simulated just for one single geographic area, e.g. limiting to 6 different temperature profiles.

Table 2
Average characteristics of trips in Italy during 2019.

	Weekday	Weekend
Average number of trips per day [–]	2.5	2.5
Average length of trips [km]	11.2	14.1
Fraction of urban trips [%]	73.9	72.6
Fraction of extra-urban trips [%]	26.1	27.4
Per capita time on mobility per day, mobile population only [min]	58	61
Average speed [km/h]	29	34
Average speed of extra-urban car journeys [km/h]	22	
Average speed of urban car journeys [km/h]	52	
Fraction of trips during peak times (7–19 and 17–19) [%]	37.7	32.3
Fraction of trips during other times [%]	62.3	67.7
Fraction of trips by car [%]	62.5	65.6
Fraction of trips by other means (including public transport) [%]	37.5	34.4

Table 3
Vehicle parameters.

Parameter	Value
Mass m	1700 kg
Wheel radius	0.34 m
Gear ratio	7
Aerodynamic coefficient C_x	0.27
Equivalent Frontal Section S	2 m^2
Rolling resistance coefficient f	0.015

Table 4
Parameters of the BESS degradation model, calibrated on the experimental tests performed using the procedure in Section 3.4.

Symbol	Value	Symbol	Value
α^{sei}	0 [–]	β^{sei}	0 [–]
$k^{\delta 1}$	1.8716E−4 [–]	$k^{\delta 2}$	4.0585 [–]
$k^{\delta 3}$	8.6848E−6 [–]	k^{σ}	0.6835 [–]
σ^{ref}	0.5 [–]	k^{T}	5.9965E−2 [–]
T^{B}_{ref}	25 [C]	k^{t}	2.835E−10 [s^{-1}]

3.4. Aging test

Several aging test have been performed on lithium-ion cell for EV application in order to get enough results to build the electrical model described in subsection Section 2.2 and the degradation model here detailed. In particular, nine NMC pouch cells manufactured by EIG, model ePLB C020B, have been tested for 2 years. The cells have a nominal capacity of 20 Ah, a voltage range between 3 and 4.15 V, a maximum charge current of 20 A and discharge current up to 60 A. The manufacturer declares more than 3000 equivalent cycles at 20 °C with DoD 80%. Fig. 11 shows the working station used for testing all the cells at the same time. It was equipped with a bidirectional multi-channel cycler, Chroma 17212R-5-100, with 12 independent channels. Two cells were tested at 40 °C in a climate chamber of Angelantoni Discovery, model DY250 BT, while seven cells were located in a steel box at 20 °C. In all the cases, the ambient temperature was kept within +/- 2 °C.

The test procedure described in [55] has been used to create a useful dataset for building a degradation model.

3.5. Degradation model

The parameters of the battery degradation model, calibrated using the experimental data obtained from the aging test and the procedure in [21], summarized in Section 2.3.4, are reported in Table 4.

Moreover, in order to clarify the contribution to the battery degradation by (a) the seasonalities of the ambient temperature and (b) the C-rate dynamics of the proposed model, in this study we compare the following three degradation models:

1. Full: the complete proposed model as described in Section 2;
2. No C-rate: the model described in Section 2 where the battery is assumed to be kept constantly at the ambient temperature, which means, no C-rate dynamics are considered;
3. AvgTemp: the model described in Section 2 where the battery is assumed to kept at the average yearly temperature throughout the year, which is the general assumption typically done in the literature [21].

Fig. 11. Working station used to perform the aging test on lithium-ion cells.

3.6. Setup of the simulations

To summarize, the characteristics of the simulations performed in this study are described in Table 5.

4. Results

This section describes the results of the proposed approach, detailed in Section 2, on the case study discussed in the previous section calibrated using the aging tests described in Section 3.4. The next subsection details the physical thermo-electric simulations of the system, developed in Modelica, and the other subsections detail the degradation behavior of the system.

Table 5
Main characteristics of the simulations.

Case	Vehicle usage	Recharge type	V2G	Weather	Degradation model
1	Commuter (30 km/d)	3 kW home	no	B/E/F	Full/No-Crate/TempAvg
2	Commuter (30 km/d)	11 kW work	no	E	Full/No-Crate/TempAvg
3	Commuter (30 km/d)	11 kW work	yes	E	Full/No-Crate/TempAvg
4	Highway (500 km/d)	120 kW+home	no	E	Full/No-Crate/TempAvg

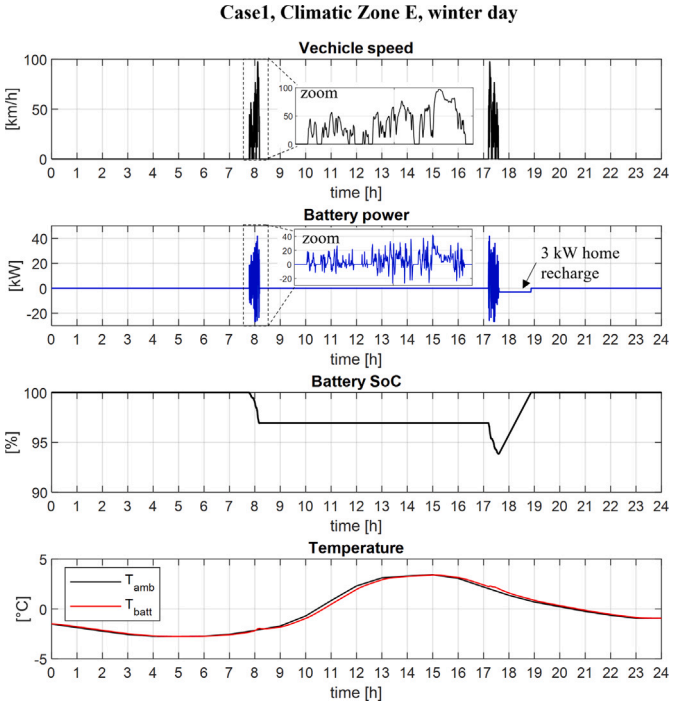

Fig. 12. Case 1, Climatic Zone E, winter day.

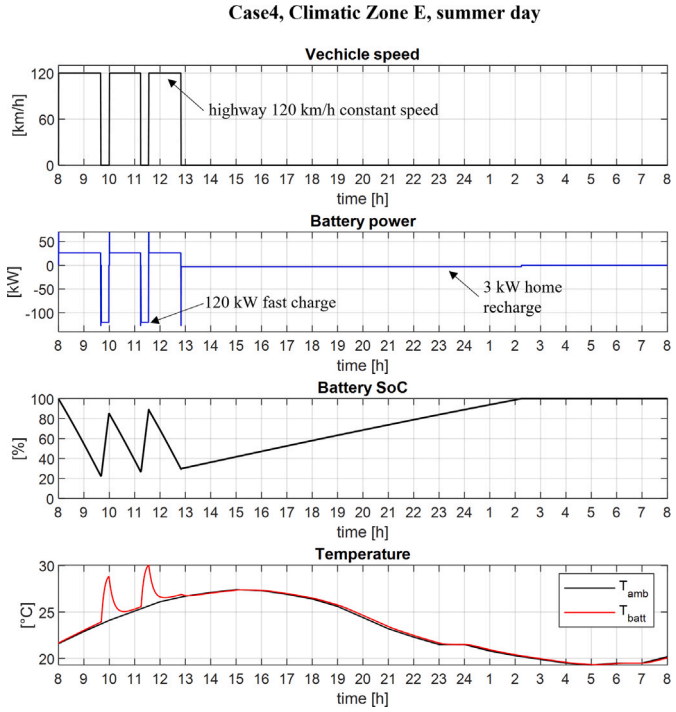

Fig. 13. Case 4, Climatic Zone E, summer day.

4.1. Thermal simulation of the vehicle battery system

As previously discussed, the thermal behavior of the vehicle battery system depends on various factors, such us the driving pattern, the battery power during traction and recharge, as well as the ambient temperature. By means of the developed simulation model, it is investigated the thermal behavior of the vehicle battery under different use cases and ambient temperature variation. This section shows the temperature variation of the vehicle battery with regard to the vehicle usage, recharge rate and ambient temperature. The trend results of two use cases for the climate zone E are depicted. In particular, Fig. 12 depicts the behavior of the battery for Case 1, during a winter day. As shown, the SoC variation is very limited, since the car travels just for 30 km per day with moderate speed. It is interesting to notice that the slow recharge at 3 kW does not affect the battery temperature which follows the ambient temperature trend. By contrast, the battery thermal profile under Case 4 is very different. As reported in Fig. 13, the battery is subjected to important SoC variation, due to higher distances and speed regime. During the drive at a constant speed of 120 km/h, the battery delivers around 26 kW and the temperature remains aligned with the ambient temperature. During the recharge phase, it is clear how the higher power level affects the battery temperature which increases by 5–6 °C with respect to the ambient.

4.2. Degradation by recharging strategy

Fig. 14 describes the expected degradation of the battery for the selected 4 usage cases (1–4) in the same climate zone E (average temperature of 18.5 °C). The image clearly shows that the different usage case, namely commuter (cases 1–3) and highway (case 4), and the intensity

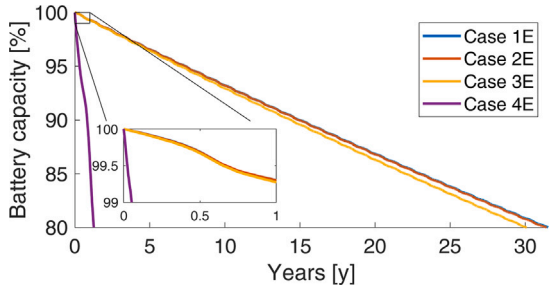

Fig. 14. Degradation of the case studies 1E, 2E, 3E and 4E at 80% DoD subject to different battery recharging patterns.

of the recharging system, from slow (case 1) to fast (case 4), can affect the lifetime of the battery. The image clearly shows that in the typical behavior of a commuter (cases 1–3) the battery vehicle is less stressed than in the highway case (4), which leads to expected lifetime of around 25 years in the cases 1–4, whereas of around 2 years in the usage case 4. However, the lifetime in terms of total kilometers driven is comparable: around 300 10^3 km in all cases, as confirmed in Table 7, the commuter case leading the way. In fact, while the battery lasts around 20 times more in terms of time in the commuter (cases 1–3), the daily kilometers covered every day in the commuter case (30 km a day) are less than one tenth of those covered in the highway case (500 km a day).

In specific, for the commuter case, the slower recharging during the night (case 1) enables improving the battery lifetime the most up to 32y, or around 340 10^3 km, at 80% conventional EoL, yet faster recharging

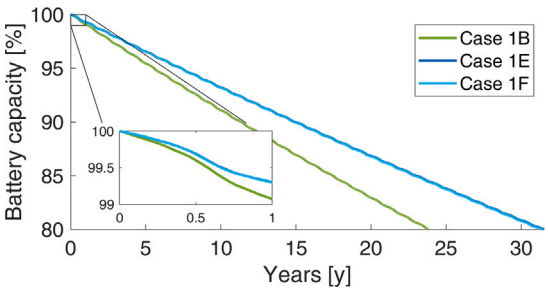

Fig. 15. Degradation of the case studies 1B, 1E and 1F at 80% DoD subject to different climate zones (B, E and F).

processes at 11 kW slightly drop lifetime by around 0.3% and 4.5% for cases 2 and 3, with respect to case 1, as shown in Fig. 14. The main reason of the drop is related to (a) increased temperature due to faster recharging processes (cases 2 and 3) and (b) increased battery cycling during V2G (only case 3).

4.3. Degradation by weather zone

In Fig. 15, the sensitivity analysis over the meteorological zones (zones B, E and F) are compared for the usage case 1, as explained in the case study. The picture clearly shows that despite the usage case is the same (case 1), the temperature affects aging for up to 24.4%: the colder temperatures (zones E and F) enable the battery to survive 24.4% longer than in the warmer regions of Southern Italy (zone B). With colder weather, the effects of the calendar aging, taken into considerations with the improvements in Section 2.3, are reduced. On the other hand, since zones E and F are similar, the corresponding degradation is nearly equivalent, as suggested by the two overlapping lines in Fig. 15.

It is interesting to notice in the zoomed area of Fig. 15 the "S"-like curve of the degradation, which is due to the monthly periodicity in the temperature. During summer, in fact, the higher temperatures lead the battery to age faster than during the winter and this is reflected by a steeper degradation during the same time period. In particular, while colder temperatures facilitate longer calendar life, the cycling life is instead more affected (see Section 2.3). However, since in the usage case 1 the battery is not significantly stressed, as the corresponding DoD is only 6%, the calendar aging is expected to play the major role in this case, as confirmed by the results in Fig. 15.

4.4. Degradation by dynamic thermal modeling

Table 6 denotes the benefits of using the proposed C-rate degradation model combined with the physical thermo-electric simulations of the vehicle system to estimate the lifetime of the batteries (first column) versus simplified methodologies to address the temperature: the model without the C-rate dynamics (second column), hence assuming the battery is constantly kept at ambient temperature, or its approximation (third column) that assumes only the average yearly temperature, as done in [21] that disregards daily and seasonal dynamics. It turns out that considering only the average yearly temperature generally leads to overestimating the battery lifetime by about 1%–18%, in most scenarios, except the coldest one (case B). The model without C-rate dynamics but that considers the seasonalities (second column) is similar to the proposed approach in cases 1–3 with low stress, but in the high-power conditions of the highway case (case 4), the higher power charging and discharging process leads the battery to significantly increase in temperature which leads to an incremental degradation loss of about 12%, which would be neglected without the proposed approach. These results suggest that seasonal dynamics shall be considered for estimating battery lifetime and that the proposed dynamic C-rate modeling is strongly recommended for estimating the battery lifetime of high power intensity conditions.

Table 6
Expected lifetime of the battery storage by thermal degradation model, case and weather zone; see Section 3.5 for the description of the acronyms of the battery degradation models.

Deg. model Case	Full[a] [10^3 km]	No C-rate [10^3 km]	AvgTemp [10^3 km]
1E	345.2	345.0 (−0.1%)	406.7 (+17.8%)
2E	344.1	343.9 (−0.1%)	408.3 (+18.7%)
3E	329.6	329.8 (+0.1%)	389.5 (+18.2%)
4E	230.8	203.3 (−11.9%)	223.2 (−3.3%)
1B	260.8	260.8 (−0.0%)	245.6 (−5.8%)
1F	343.8	343.5 (−0.1%)	437.9 (+27.3%)

[a]Proposed model and reference case.

Table 7
Expected lifetime of the battery storage by End-of-Life; units are in years.

		Time [y]	Time [y]	Path [10^3 km]	Path [10^3 km]
EoL [%]		80	70[a]	80	70[a]
Case	1E	31.5	49.8	345.2	545.8
	2E	31.4	49.6	344.1	543.1
	3E	30.1	47.5	329.6	520.2
	4E	1.3	1.8	230.8	335.8
	1B	23.8	38	260.8	415.6
	1F	31.4	49.6	343.8	543.2

[a]Assuming no second-life phenomena kick-in.

4.5. Effect of the End of Life (EoL)

Table 7 shows the expected lifetime of the battery, both in terms of years of operation and total path covered, of the vehicle for all usage conditions (cases 1–4) and tested weather zones, also including a sensitivity analysis over the conventional EoL of the battery (80% and 70%), under the assumption that no second-life behaviors occur. Increasing the conventional EoL of the battery from 80% to 70% enables increasing the timespan by around 15 years. However, it is worth noticing that after these long lifespan and deep discharges, non-linearities related to second-life behavior, which are not the focus of this study, are more likely to kick in than at 80% EoL.

5. Conclusions

This study has successfully proposed a methodology to estimate the lifetime expectancy of electric vehicle battery systems subject to arbitrary weather conditions, vehicle uses and charging strategies, including fast charging, vehicle-to-grid and home recharge. A novel rainflow-based degradation model has been proposed and calibrated to consider cold and warm environments, the effects of the C-rate, the temperature-related calendar life and resting periods, alongside with the traditional cycling degradation performances. A physical-electro-thermal model of the vehicle system has been included to cope with the C-rate dynamics of the battery usage.

The results suggest that lifetimes in the range of 10–20y (200–300 10^3km) are realistic for vehicle battery systems used by commuters with expected daily usage in the range of 30 km a day, regardless of the weather zone, as compared with commercial data and other studies. More heavy usage of the battery, such as in highway conditions, can lead to drop in the expected calendar lifetime in the range of 1–2y, but limited reductions in terms of total traveled kilometers, with respect to the average commuter.

Results suggest that accurate temperature and C-rate modeling are required to avoid estimation errors beyond 18%–27% in the battery lifetime expectancy, especially when approximating the battery dynamics to the average yearly value. The C-rate related effects have shown to impact battery estimation lifetime up to 12% for the highway case, as the heavier charging and discharging processes lead to increased battery

temperatures. Therefore, results suggest modelers to account for C-rate considerations to properly estimate the lifetime of vehicle battery systems.

Further studies shall address the suitability of the model for different battery chemistries, supported by large experimental data, and the possible interaction of the vehicle battery system with the recharging station, to account for the degradation costs during the recharging process.

CRediT authorship contribution statement

Davide Fioriti: Conceptualization, Methodology, Software, Investigation, Data curation, Writing – original draft, Writing – review & editing, Visualization, Supervision. **Claudio Scarpelli:** Software, Investigation, Data curation, Writing – original draft. **Luigi Pellegrino:** Conceptualization, Methodology, Resources, Writing – original draft, Writing – review & editing, Project administration, Funding acquisition. **Giovanni Lutzemberger:** Methodology, Software, Writing – review & editing, Visualization, Supervision. **Enrica Micolano:** Conceptualization, Writing – original draft. **Sara Salamone:** Data curation, Writing – original draft.

Declaration of competing interest

The authors declare that they have no known competing financial interests or personal relationships that could have appeared to influence the work reported in this paper.

Data availability

Data will be made available on request.

Acknowledgments

This work has been funded by the Research Fund for the Italian Electrical System under the Contract Agreement between RSE S.p.A. and the Ministry of Economic Development - General Directorate for the Electricity Market, Renewable Energy and Energy Efficiency, Nuclear Energy in compliance with the Decree of April 16th, 2018.

References

[1] P. Chakraborty, R. Parker, T. Hoque, J. Cruz, L. Du, S. Wang, S. Bhunia, Addressing the range anxiety of battery electric vehicles with charging en route, Sci. Rep. 12 (1) (2022) 1–15.

[2] S. Lee, J. Cherry, M. Safoutin, J. McDonald, M. Olechiw, Modeling and validation of 48V mild hybrid lithium-ion battery pack, SAE Int. J. Alternative Powertrains 7 (3) (2018) 273–288.

[3] M.S. Lipu, M.A. Hannan, A. Hussain, M.M. Hoque, P.J. Ker, M.H. Saad, A. Ayob, A review of state of health and remaining useful life estimation methods for lithium-ion battery in electric vehicles: Challenges and recommendations, J. Clean. Prod. 205 (2018) 115–133.

[4] A. Pena-Bello, E. Barbour, M.C. Gonzalez, M.K. Patel, D. Parra, Optimized PV-coupled battery systems for combining applications: Impact of battery technology and geography, Renew. Sustain. Energy Rev. 112 (February) (2019) 978–990.

[5] R.T. Yadlapalli, A. Kotapati, R. Kandipati, C.S. Koritala, A review on energy efficient technologies for electric vehicle applications, J. Energy Storage 50 (February) (2022) 104212.

[6] Y. Ding, Z.P. Cano, A. Yu, J. Lu, Z. Chen, Automotive Li-ion batteries: Current status and future perspectives, Electrochem. Energy Rev. 2 (1) (2019) 1–28.

[7] A. Kwade, W. Haselrieder, R. Leithoff, A. Modlinger, F. Dietrich, K. Droeder, Current status and challenges for automotive battery production technologies, Nature Energy 3 (4) (2018) 290–300.

[8] I. Laresgoiti, S. Käbitz, M. Ecker, D.U. Sauer, Modeling mechanical degradation in lithium ion batteries during cycling: Solid electrolyte interphase fracture, J. Power Sources 300 (2015) 112–122.

[9] M. Jafari, K. Khan, L. Gauchia, Deterministic models of Li-Ion battery aging: It is a matter of scale, J. Energy Storage 20 (2018) 67–77.

[10] M. Ceraolo, G. Lutzemberger, D. Poli, Aging evaluation of high power lithium cells subjected to micro-cycles, J. Energy Storage 6 (2016) 116–124.

[11] W. Diao, S. Saxena, M. Pecht, Accelerated cycle life testing and capacity degradation modeling of LiCoO2-graphite cells, J. Power Sources 435 (June) (2019) 226830.

[12] M. Berecibar, I. Gandiaga, I. Villarreal, N. Omar, J. Van Mierlo, P. Van Den Bossche, Critical review of state of health estimation methods of Li-Ion batteries for real applications, Renew. Sustain. Energy Rev. 56 (2016) 572–587.

[13] B.Y. Liaw, E.P. Roth, R.G. Jungst, G. Nagasubramanian, H.L. Case, D.H. Doughty, Correlation of Arrhenius behaviors in power and capacity fades with cell impedance and heat generation in cylindrical lithium-ion cells, J. Power Sources 119–121 (2003) 874–886.

[14] J. Wu, Z. Wei, W. Li, Y. Wang, Y. Li, D.U. Sauer, Battery thermal- and health-constrained energy management for hybrid electric bus based on soft actor-critic DRL algorithm, IEEE Trans. Ind. Inform. 17 (6) (2021) 3751–3761.

[15] M. Yue, S. Jemei, R. Gouriveau, N. Zerhouni, Review on health-conscious energy management strategies for fuel cell hybrid electric vehicles: Degradation models and strategies, Int. J. Hydrogen Energy 44 (13) (2019) 6844–6861.

[16] H. Tian, P. Qin, K. Li, Z. Zhao, A review of the state of health for lithium-ion batteries: Research status and suggestions, J. Clean. Prod. 261 (2020) 120813.

[17] N. Omar, M.A. Monem, Y. Firouz, J. Salminen, J. Smekens, O. Hegazy, H. Gaulous, G. Mulder, P. Van den Bossche, T. Coosemans, J. Van Mierlo, Lithium iron phosphate based battery - Assessment of the aging parameters and development of cycle life model, Appl. Energy 113 (2014) 1575–1585.

[18] G. Suri, S. Onori, A control-oriented cycle-life model for hybrid electric vehicle lithium-ion batteries, Energy 96 (2016) 644–653.

[19] X. Han, M. Ouyang, L. Lu, J. Li, A comparative study of commercial lithium ion battery cycle life in electric vehicle: Capacity loss estimation, J. Power Sources 268 (2014) 658–669.

[20] J. Cannarella, C.B. Arnold, Stress evolution and capacity fade in constrained lithium-ion pouch cells, J. Power Sources 245 (2014) 745–751.

[21] B. Xu, A. Oudalov, A. Ulbig, G. Andersson, D.S. Kirschen, Modeling of lithium-ion battery degradation for cell life assessment, IEEE Trans. Smart Grid 9 (2) (2018) 1131–1140.

[22] L. Lam, P. Bauer, Practical capacity fading model for Li-ion battery cells in electric vehicles, IEEE Trans. Power Electron. 28 (12) (2013).

[23] D. Fioriti, MDO-PSO, 2022, URL https://github.com/davide-f/MDO-PSO.

[24] ASTM E1049-85, Standard Practices for Cycle Counting in Fatigue Analysis, Tech. Rep., ASTM International, 2017.

[25] T. Wang, C. Li, L. Chang, B. Duan, C. Zhang, Thermal behavior analysis of pouch lithium ion battery using distributed electro-thermal model, in: 2019 3rd Conference on Vehicle Control and Intelligence, CVCI, 2019, pp. 1–5.

[26] J. Kleiner, A. Heider, C. Hanzl, L. Komsiyska, G. Elger, C. Endisch, Thermal behavior of an intelligent Li-ion cell under vehicle conditions, in: IECON 2020 the 46th Annual Conference of the IEEE Industrial Electronics Society, 2020, pp. 2081–2086.

[27] R. Yang, K. Li, Y. Xie, W. Li, Y. Qian, Y. Zhang, H. Zhang, Thermal management of a 48 V lithium-ion battery pack by semiconductor refrigeration, Front. Energy Res. 9 (2022).

[28] S. Tang, Z. Wang, H. Guo, J. Wang, X. Li, G. Yan, Systematic parameter acquisition method for electrochemical model of 4.35 V LiCoO2 batteries, Solid State Ion. 343 (2019) 115083.

[29] D. Bernardi, E. Pawlikowski, J. Newman, A general energy balance for battery systems, J. Electrochem. Soc. 132 (1) (1985) 5–12.

[30] Y. Preger, H.M. Barkholtz, A. Fresquez, D.L. Campbell, B.W. Juba, J. Romàn-Kustas, S.R. Ferreira, B. Chalamala, Degradation of commercial lithium-ion cells as a function of chemistry and cycling conditions, J. Electrochem. Soc. 167 (12) (2020) 120532.

[31] S. Atalay, M. Sheikh, A. Mariani, Y. Merla, E. Bower, W.D. Widanage, Theory of battery ageing in a lithium-ion battery: Capacity fade, nonlinear ageing and lifetime prediction, J. Power Sources 478 (2020) 229026.

[32] T.A. Lehtola, A. Zahedi, Electric vehicle battery cell cycle aging in vehicle to grid operations: A review, IEEE J. Emerg. Sel. Top. Power Electron. 9 (1) (2019) 423–437.

[33] G. Saldaña, J.I. San Martín, I. Zamora, F.J. Asensio, O. Onederra, M. González, Empirical electrical and degradation model for electric vehicle batteries, IEEE Access 8 (2020) 155576–155589.

[34] Volkswagen Official site, 2022, https://www.volkswagenag.com/en/news/stories/2019/04/our-batteries-last-the-life-of-a-car.html. (Accessed 06 May 2022).

[35] Tesla Official site, 2022, https://www.tesla.com/support/vehicle-warranty.html. (Accessed 06 May 2022).

[36] Reanult Official site, 2022, https://www.renaultgroup.com/en/news-on-air/news/how-does-the-renault-zoe-batterys-warranty-work.html/. (Accessed 06 May 2022).

[37] P. Fritzson, Introduction to Modeling and Simulation of Technical and Physical Systems with Modelica, John Wiley & Sons, 2011.

[38] J. Li, G. Lutzemberger, D. Poli, C. Scarpelli, T. Piazza, Simulation and experimental validation of a hybrid forklift truck, in: 2019 AEIT International Conference of Electrical and Electronic Technologies for Automotive, AEIT AUTOMOTIVE, 2019, pp. 1–6.

[39] M. Ceraolo, G. Lutzemberger, C. Scarpelli, G.P. Bonelli, T. Piazza, Hybridisation of forklift trucks, IET Electr. Syst. Transport. 10 (1) (2020) 116–123.

[40] M. Barbieri, M. Ceraolo, G. Lutzemberger, C. Scarpelli, An electro-thermal model for LFP cells: Calibration procedure and validation, Energies 15 (7) (2022).

[41] R.R. Thakkar, Y. Rao, R. R.Sawant, Performance analysis of electrical equivalent circuit models of lithium-ion battery, in: 2020 IEEE Pune Section International Conference, PuneCon, 2020, pp. 103–107.
[42] M. Barbieri, M. Ceraolo, G. Lutzemberger, C. Scarpelli, T. Pesso, M. Giovannucci, Simplified electro-thermal model for lithium cells based on experimental tests, in: 2020 AEIT International Conference of Electrical and Electronic Technologies for Automotive, AEIT AUTOMOTIVE, 2020, pp. 1–6.
[43] C. Zhang, X. Jin, J. Li, PTC self-heating experiments and thermal modeling of lithium-ion battery pack in electric vehicles, Energies 10 (4) (2017).
[44] L. Fan, J. Khodadadi, A. Pesaran, A parametric study on thermal management of an air-cooled lithium-ion battery module for plug-in hybrid electric vehicles, J. Power Sources 238 (2013) 301–312.
[45] S. Wijewardana, R. Vepa, M. Shaheed, Dynamic battery cell model and state of charge estimation, J. Power Sources 308 (2016) 109–120.
[46] M. Alhanouti, M. Gießler, T. Blank, F. Gauterin, New electro-thermal battery pack model of an electric vehicle, Energies 9 (7) (2016).
[47] L. Saw, K. Somasundaram, Y. Ye, A. Tay, Electro-thermal analysis of lithium iron phosphate battery for electric vehicles, J. Power Sources 249 (2014) 231–238.
[48] D. Fioriti, L. Pellegrino, G. Lutzemberger, E. Micolano, D. Poli, Optimal sizing of residential battery systems with multi-year dynamics and a novel rainflow-based model of storage degradation: An extensive Italian case study, Electr. Power Syst. Res. 203 (March 2021) (2022) 107675.
[49] T. Waldmann, M. Wilka, M. Kasper, M. Fleischhammer, M. Wohlfahrt-Mehrens, Temperature dependent ageing mechanisms in lithium-ion batteries - A Post-Mortem study, J. Power Sources 262 (2014) 129–135.
[50] J. Jaguemont, L. Boulon, Y. Dubé, A comprehensive review of lithium-ion batteries used in hybrid and electric vehicles at cold temperatures, Appl. Energy 164 (2016) 99–114.
[51] L. Croci, S. Viani, G. Besagni, L. Rota, F. Ravasio, R. Menga, F. Bazzocchi, Fabbisogno Di Climatizzazione Invernale Ed Estiva Degli Edifici Residenziali E Del Terziario, Tech. Rep RdS 18007687, Ricerca sul Sistema Energetico, 2018.
[52] WLTC cycle, 2022, https://dieselnet.com/standards/cycles/wltp.php. (Accessed 20 April 2022).
[53] Isfort Report 2020, 2022, https://www.isfort.it/wp-content/uploads/2020/12/RapportoMobilita2020.pdf. (Accessed 20 April 2022).
[54] Electric vehicle database, 2022, https://ev-database.org. (Accessed 20 October 2022).
[55] L. Pellegrino, E. Micolano, Aging test protocol for lithium-ion cells, in: 2019 AEIT International Annual Conference, AEIT, 2019, pp. 1–6.